

Rathole Stability Analysis for Aerated Powder Materials

By: Dr. Kerry Johanson Material Flow Solutions, Inc.

NOTICE: This is the author's version of a work accepted for publication by Elsevier. Changes resulting from the publishing process, including peer review, editing, corrections, structural formatting and other quality control mechanisms, may not be reflected in this document. Changes may have been made to this work since it was submitted for publication. A definitive version was subsequently published in Powder Technology, Vol. 141, 17 April 2004, Pages 161-170, doi:10.1016/j.powtec.2004.02.004.

Abstract:

Forty years ago Jenike and Johanson developed the flow-no-flow equations used to predict stability of bulk solid structures in silos and hoppers. These equations were developed into a theory that has been used to design process equipment to handle cohesive materials. The basis of the theory is a limiting stress state analysis of a bulk material forming a cylindrical pipe (rathole) around or an arch across the hopper outlet. Reliable process operation requires that these two cohesive obstructions be avoided to achieve proper flow of bulk materials through process equipment. Today, industry uses a variety of flow aid devices to overcome these stable flow structures. One such device is aeration pads which are used to maintain fluidization of fine powders and decrease cohesive behavior of bulk materials. Alternatively, air blasters can inject a given quantity of gas into the bulk material creating large transient gas pressure gradients that may destroy these cohesive structures in process equipment. It is important to note that air blasters may destroy cohesive structures provided they are placed in close enough proximity to the stable rathole and with sufficient frequency along the axis of the bin or around the bin perimeter. Although these aeration techniques work, a full understanding of the reason is lacking. Currently, both the placement and required number of these flow aid devices are based on practical experience and not sound theoretical principles. This paper addresses this knowledge void by adding the gas pressure gradient terms to the rathole stability analysis performed by Jenike, thus extending the flow-no-flow rathole analysis to aerated conditions.

Key Words: rathole, slope stability, cohesion, unconfined yield strength, aeration

Introduction:

Processing and handling of fine materials is often difficult. These materials sometimes behave as cohesive masses. However, the addition of air often creates a condition wherein bulk materials exhibit less cohesive tendencies. One example of using aeration to overcome cohesive flow problems is the use of air pads in flat-bottom ash silos to keep material in a flowable condition. Standard rules of thumb suggest that a minimum of 15% of the silo bottom should be covered with air pads to maintain ash in a flowable state. Air flow should be used during filling and maintained during storage. Since a sound theory of cohesive aerated behavior does not exist, current bulk solids practitioners' err on the side of safety and often recommend that the entire bottom be fluidized with the hope that more aeration will provide some safety margin for design. The placement of these pads is more art than science and the amount of air injected is empirical and based on past experience. If the injection system fails, the material within the silo loses entrained gas and cohesive ratholes result. The relationship between rathole stability and degree of aeration is not well understood. This paper addresses a theoretical approach for stable rathole formation in aerated hoppers and bins. It is an extension of the critical rathole stability criteria initially proposed by Jenike [1].

Two conditions that must be satisfied for trouble free process operations using powder materials are that the outlet must be large enough to overcome cohesive arching of bulk materials and that the active flow channel must be larger than the critical rathole dimension. The Jenike arching criteria equations [1] [2] are often used to compute the arching tendency. Alternatively, the arching index approach [3] is used to compute critical arching dimensions. However, reliable flow of bulk material from process equipment also requires that the induced flow channel be large enough to prevent the formation of stable ratholes. Jenike also developed a limiting stress state analysis for prediction of critical rathole diameters in funnel flow bins. This method has been used with moderate success over the last 40 years to provide a conservative estimate of the critical rathole diameter. However it does have some limitations.

APPLICATION NOTE 013

This paper attempts to address one of these limitations.

Both the arching and rathole conditions must be overcome to assure reliable flow. This paper focuses on only the rathole tendency of bulk powders and deals directly with the influence of aeration on the ability of a powder material to form a stable rathole. It will leave the formation of arches in aerated material to some future work. It should be noted that, quite often, in funnel flow bins the critical rathole dimension is the controlling factor in successful handling system operation. The rathole flow-no-flow criteria states that the active flow channel induced in the material must be greater than the critical rathole dimension for reliable flow to occur. The question then arises as to how this critical diameter changes during powder aeration. Two things are required to determine the effect of aeration on cohesive flow obstructions. The relationship between aeration and cohesive flow properties must be established and the stability of cohesive structures under aeration conditions must be understood.

Recent work by Barletta [4], Johanson and Barletta [5], and Kline et. al. [6] makes measurement of unconfined yield strength as a function of aeration possible. These aerated flow property measurements can be used to predict critical rathole dimensions for aerated process equipment. Their work suggests there is a relationship between aeration and unconfined yield strength. However, this effect does not become a dominant issue until the gas pressure gradient acting in the powder approaches the weight density of the bulk powder.

From a theoretical point of view Hill and Cox [7] analyzed the limiting stability rathole equations but did not include gas pressure terms. There is limited discussion in their paper about the validity of their new critical rathole dimension predictions and they neglected to add the gas pressure gradient terms. Hence, their analysis can not handle aerated materials. The following paper addresses the rathole stability in aerated conditions and presents an analysis similar to the one proposed by Jenike, except it includes gas pressure gradient terms.

Derivation of the critical rathole equations

The rathole derivation as defined by Jenike is a critical slope stability calculation and assumes a perfectly plastic limit analysis. The governing equation is called the equilibrium equation and is simply the equation of motion with the acceleration terms omitted (see Eq. 1).

$$\nabla \cdot \underline{\tau} = \gamma \underline{g} - \nabla P \quad (1)$$

This results in the following vector component equations when expressed in cylindrical coordinates see Figure 1.

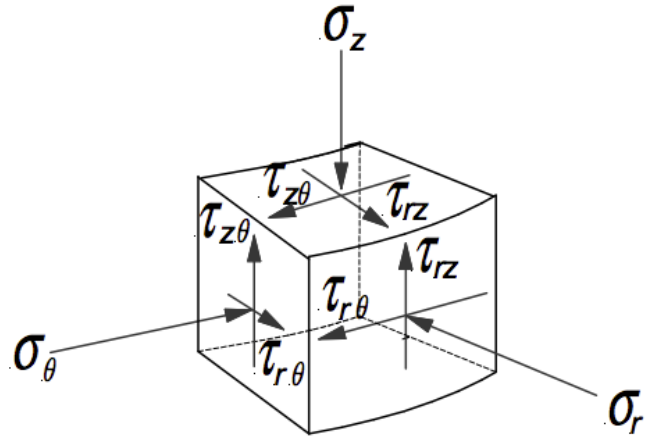


Figure 1: Definition of stress components

$$\frac{1}{r} \cdot \frac{\partial(r \cdot \sigma_r)}{\partial r} + \frac{1}{r} \cdot \frac{\partial(t_{r\theta})}{\partial \theta} - \frac{\sigma_\theta}{r} + \frac{\partial(t_{rz})}{\partial z} = -\frac{\partial P}{\partial r} + \gamma \cdot g_r \quad (2)$$

$$\frac{1}{r} \cdot \frac{\partial(r \cdot t_{rz})}{\partial r} + \frac{1}{r} \cdot \frac{\partial(t_{\theta z})}{\partial \theta} + \frac{\partial(\sigma_z)}{\partial z} = -\frac{\partial P}{\partial z} + \gamma \cdot g_z \quad (3)$$

Normal stress in the θ -direction is assumed to equal the major principal stress in accordance with the Har Von Karman hypothesis, which states that the hoop stress in bulk material is equal to either the major or minor principal stress. This assumption implies that the shear stresses $\tau_{r\theta}$ and $\tau_{\theta z}$ equal zero. The critical rathole dimension for a given piece of process equipment should depend on the strength evaluated at the greatest solids contact stress in the equipment. Janssen [8] analyzed the stresses in cylindrical silos and found an asymptotic relationship for the stress as a function of the axial coordinate. In a silo, the largest solids stress occurs far below the top material surface. At this location, the Janssen stress profile produces a condition where the normal stress σ_z is constant with bed depth. Hence, the terms $M\sigma_z/Mz$ and $M\tau_{rz}/Mz$ equal zero. These assumptions result in the simplified Eq. 4 and Eq. 5.

$$\frac{1}{r} \cdot \frac{\partial(r \cdot \sigma_r)}{\partial r} - \frac{\sigma_\theta}{r} = -\frac{\partial P}{\partial r} \quad (4)$$

$$\frac{1}{r} \cdot \frac{\partial(r \cdot t_{rz})}{\partial r} = -\frac{\partial P}{\partial z} + \gamma \cdot g_z \quad (5)$$

APPLICATION NOTE 013

These equations are transformed using the scale variable proposed in the original rathole analysis. This transformation relates the radial position to a new variable η as given by Eq. 6 and Figure. 2.

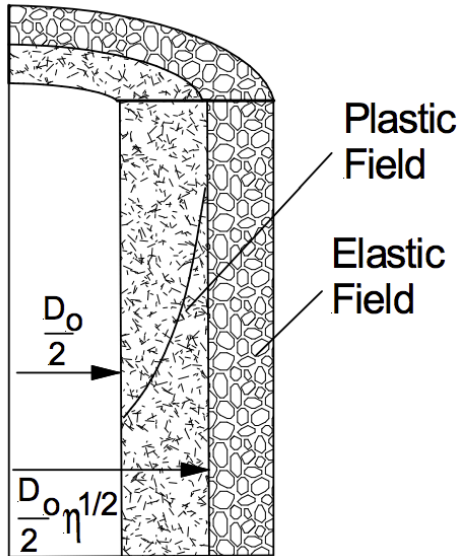


Figure 2: Rathole schematic

$$r = \frac{1}{2} \cdot \eta^{1/2} \cdot D_0 \quad (6)$$

The new rathole stability equations become the following:

$$\frac{d\sigma_r}{d\eta} + \frac{\sigma_r - \sigma_\theta}{2 \cdot \eta} = - \frac{\partial P}{\partial r} \cdot \frac{D_0}{4 \cdot \eta^{1/2}} \quad (7)$$

$$\frac{dt_{rz}}{d\eta} + \frac{t_{rz}}{2 \cdot \eta} = \left[\gamma \cdot g_z - \frac{\partial P}{\partial r} \right] \quad (8)$$

They are similar to the equations originally derived by Jenike, but include gas pressure gradient terms. Eq. 8 can be integrated directly, subject to the boundary condition of zero shear stress at the rathole surface and nearly constant gas pressure gradient in the axial direction, to yield Eq. 9 describing the shear stress as a function of radial position away from the rathole surface.

$$t_{rz} = \frac{1}{4} \cdot \left[\gamma \cdot g_z - \frac{\partial P}{\partial z} \right] \cdot D_0 \cdot \frac{(\eta-1)}{\eta^{1/2}} \quad (9)$$

Eq. 7 and Eq. 8 can not be solved directly, since the number of unknown variables exceeds the number of vector component equations. A constitutive equation relating the normal stresses σ_θ and σ_r is required in order to provide closure to this system of equations.

The concept of a perfect plastic material provides the necessary closure equations. When stress levels reach a critical value, yield will occur. The perfectly plastic assumption uses the stress state at the point of yield as the stress state for all plastic flow conditions. Obviously, this only applies to the condition of incipient flow or yield. Such an assumption can not hope to predict flow behavior between the incipient flow and continual deformation conditions. Consequently, the model derived from these equations may predict the incipient failure of a rathole, but will not give any information describing the flow after initiation. This limitation of the theory is acceptable for this rathole stability analysis since the goal of this work is to predict the incipient failure of a rathole. The yield locus then becomes the constitutive equation required for closure of the equation of motion. The yield locus is the collection of shear stress (τ) normal stress points (σ) that describe incipient failure of a bulk material subjected to a prescribed compaction stress. Figure 3 shows a typical yield locus. The bold line represents the collection of all stress states that will result in yield of the bulk material. This line terminates at a stress condition given by the largest Mohr circle. All failure conditions on the yield locus arise from subjecting the material to the compaction stress state described by this termination Mohr circle and then shearing the preconditioned bulk material at a lower stress state. There is an unique yield locus for each compaction stress state. A linear approximation to this yield locus provides the constitutive equation required for closure of Eqs. 7 and 8. This relationship allows the stress tensor components to be expressed as a function of the mean stress. It is also a function of the direction between the major principal stress and coordinate axis.

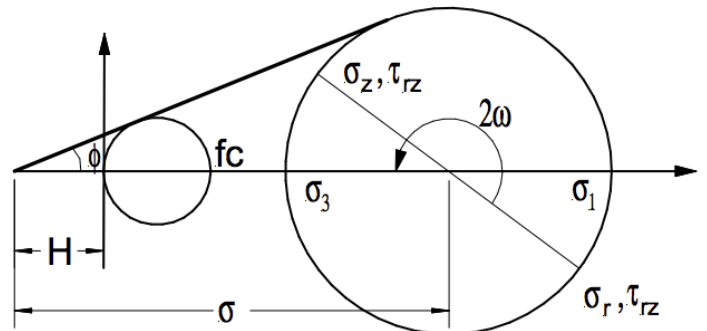


Figure 3: Definition of limiting stress state for rathole analysis

APPLICATION NOTE 013

This definition is identical to the limiting state constitutive equation used by Jenike in his original rathole analysis. It is important to note that the average stress defined in this figure is measured from the apex of the yield locus and not from the origin. This results in Eqs. 10 through 13 for the stress equations.

$$\sigma_r = \sigma \cdot [1 - \sin(\theta) \cdot \cos(2\omega)] + \frac{fc}{2} \cdot \frac{\sin(\theta) - 1}{\sin(\theta)} \quad (10)$$

$$\sigma_z = \sigma \cdot [1 + \sin(\theta) \cdot \cos(2\omega)] + \frac{fc}{2} \cdot \frac{\sin(\theta) - 1}{\sin(\theta)} \quad (11)$$

$$t_{rz} = \sigma \cdot [\sin(\theta) \cdot \sin(2\omega)] \quad (12)$$

$$\sigma_\theta = \sigma \cdot [1 + \sin(\theta)] + \frac{fc}{2} \cdot \frac{\sin(\theta) - 1}{\sin(\theta)} \quad (13)$$

Eq. 9 can be substituted back into Eq. 8 to yield a relationship between η and τ_{rz} .

$$\frac{2 \cdot \sigma \cdot \sin(\theta) \cdot \sin(2\omega) \cdot \frac{d\omega}{d\eta} + \sin(\theta) \cdot \cos(2\omega) \cdot \frac{d\sigma}{d\eta} - \frac{1}{2} \cdot \frac{1 + \cos(2\omega)}{\eta}}{\sigma \cdot \sin(\theta)} = - \frac{\frac{\partial P}{\partial r} \cdot \frac{D_0}{4 \cdot \eta^{1/2}}}{\sigma \cdot \sin(\theta)} \quad (16)$$

$$\frac{\frac{\partial P}{\partial r} \cdot \frac{D_0}{4 \cdot \eta^{1/2}}}{\sigma \cdot \sin(\theta)} = \frac{\frac{\partial P}{\partial r} \cdot \sin(2\omega)}{(\eta - 1) \cdot \left[\gamma \cdot g - \frac{\partial P}{\partial z} \right]} \quad (17)$$

The right side of Eq. 16 can be modified by using the integrated shear stress Eq. 9 and the Mohr circle definition for the shear stress in Eq. 12. This yields Eq. 17 and eliminates the mean stress term from the right side of Eq. 16. This allows

$$\frac{\partial t_{rz}}{\partial \eta} = t_{rz} \cdot \frac{\eta + 1}{\eta \cdot (\eta - 1)} \quad (14)$$

Eq. 14 can then be combined with the Mohr stress yield conditions to provide a relationship between the mean stress (σ) and principal stress direction angle (ω).

$$\frac{1}{\sigma} \cdot \frac{d\sigma}{d\eta} + 2 \cdot \frac{\cos(2\omega)}{\sin(2\omega)} \cdot \frac{d\omega}{d\eta} - \frac{(\eta + 1)}{2 \cdot \eta \cdot (\eta + 1)} = 0 \quad (15)$$

Eq. 15 provides a means of relating mean stress to the principal stress direction. It arises from the solution of the axial equation of motion subject to the simple boundary conditions and assumptions outlined above. The radial component of the equation of motion can also be expressed as a function of mean stress (σ) and principal stress direction (ω). This can be done by substituting Eqs. 10 through 13 into Eq. 7 to yield Eq. 16.

complete separation of the mean stress and principle stress direction derivatives and leads to Eq. 18, which describes the change of principle stress direction (ω) with respect to the dimensionless radial coordinate (η).

$$\frac{d\omega}{d\eta} = \frac{\sin(2\omega)}{4} \cdot \frac{[-\eta - 1 + 2 \cdot \eta \cdot \sin(\theta) \cdot \cos(2\omega) - \sin(\theta) + 2 \cdot \eta \cdot A \cdot \sin(2\omega) \cdot \sin(\theta)]}{\eta \cdot (\eta - 1) \cdot [\sin(\theta) - \cos(2\omega)]} \quad (18)$$

$$A = \frac{\frac{\partial P}{\partial r}}{\frac{\partial P}{\partial z} - \gamma \cdot g_z} \quad (19)$$

APPLICATION NOTE 013

This differential equation must be bounded within the limits of integration to produce physically realizable solutions. Therefore, an analysis of the extreme points of this equation will yield limits on the principal stress direction angle. The denominator can become unbounded if $\sin(\varphi)$ equals $\cos(2\omega)$. This results in Eq. 20 describing the maximum limit of principal stress direction angle.

$$\omega = \frac{\pi}{4} - \frac{\varphi}{2} \quad (20)$$

The numerator must also vanish at this value of ω to maintain a bounded solution. This yields a relationship between the dimensionless coordinate (η), dimensionless gas pressure gradient term (A), and internal friction angle (φ) (Eq. 21). The dimensionless coordinate η_{\max} is the largest possible radial position that can create a plastic stress field given a rathole diameter of D_0 .

$$\omega = \frac{1}{2 \cdot \sin(\varphi) - 1 + \frac{A \cdot 2 \cdot \cos(\varphi) \cdot \sin(\varphi)}{1 + \sin(\varphi)}} \quad (21)$$

The maximum radius of the plastic field is then given by Eq. 22.

$$r = \frac{D_0}{2} \cdot \eta_{\max}^{1/2} \quad (22)$$

Now at the surface of the rathole, η approaches 1, ω approaches 0, and σ_1 approaches the unconfined yield strength f_c . This implies the following relationship between unconfined yield strength (f_c) and average stress level (σ).

$$2 \cdot \sigma \cdot \sin(\varphi) = f_c \quad (23)$$

However, from the solution of the shear stress differential equation average stress can be related to the rathole diameter (D_0).

$$\frac{\sin(2\omega)}{\eta - 1} = \frac{1}{4} \frac{\left[\gamma \cdot g_z - \frac{\partial P}{\partial z} \right] \cdot D_0}{\eta^{1/2}} \quad (24)$$

Eq. 23 and Eq. 24 can be combined to yield a relationship between the rathole diameter and the direction of major principal stress near the rathole surface (Eq. 25).

$$D_0 = \lim \left[2 \cdot f_c \cdot \frac{\sin(2\omega)}{\eta - 1} \cdot \frac{\eta^{1/2}}{\gamma \cdot g_z - \frac{\partial P}{\partial z}} \right] \quad (25)$$

L'Hospital rule must be used to evaluate this limit, resulting in the following equation for the rathole diameter.

$$D_0 = \frac{4 \cdot \frac{d\omega(1)}{d\eta} \cdot f_c}{\gamma \cdot g_z - \frac{\partial P}{\partial z}} = \frac{G \cdot (\varphi, A) \cdot f_c}{\gamma \cdot g_z - \frac{\partial P}{\partial z}} \quad (26)$$

It is obvious from this equation that the derivative of the major principal stress direction, with respect to the dimensionless radial coordinate evaluated at the surface of the rathole ($\eta=1$), is required to determine a maximum limit to the critical rathole diameter. The $G(\varphi, A)$ term defined above is four times the derivative of the principal stress direction with respect to the dimensionless radial coordinate (η). It is similar to the $G(\varphi)$ term derived by Jenike, but includes gas pressure gradient terms. This derivative can be obtained by integrating Eq. 18 subject to the boundary condition $\eta=\eta_{\max}$ at $\omega=\pi/4 - \varphi/2$. Because of the complexity of the differential equation, integration must be done numerically. The integration proceeds backwards from the boundary condition at η_{\max} and terminates at $\eta=1$. The derivative of the principal stress direction angle (ω) with respect to dimensionless radial coordinate (η) evaluated at $\eta=1$ is then used to compute the critical rathole diameter. As a first approximation, gas pressure gradient terms are assumed constant. This is not strictly true and there will be some variation with both radial and axial position in the bin.

A more accurate solution should involve the combined numerical solution of the limiting rathole equations along with the equations of motion describing gas flow through powder. However, the analysis provided in this paper can provide a first approximation to rathole stability in aerated process equipment. Figure 4 shows a typical solution to the differential equation.

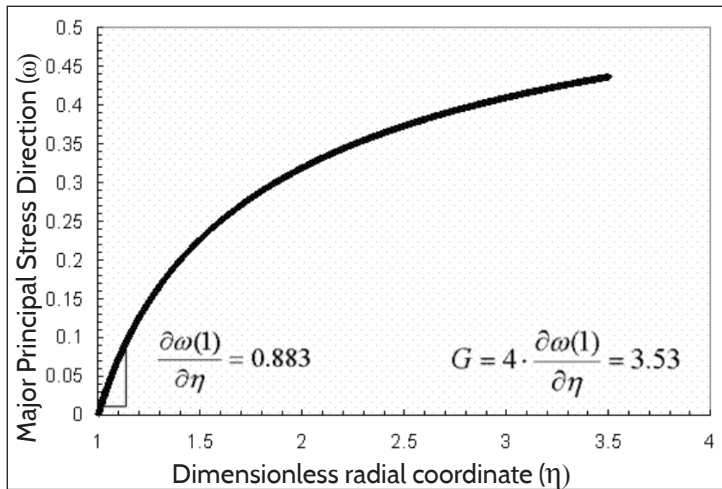


Figure 4: Typical solution for aerated rathole equation

This integration can be repeated for various values of (A) and internal angle of friction (ϕ) resulting in a new relationship for the $G(\phi, A)$ function that includes gas pressure gradient terms (Figures 5 and 6). It is important to note that the radial component of the gas pressure gradient is responsible for rathole destabilization. The larger this gas pressure gradient, the more unstable the rathole becomes. The axial gradient term actually causes the rathole to be more stable by decreasing the effective gravitational forces acting on the rathole.

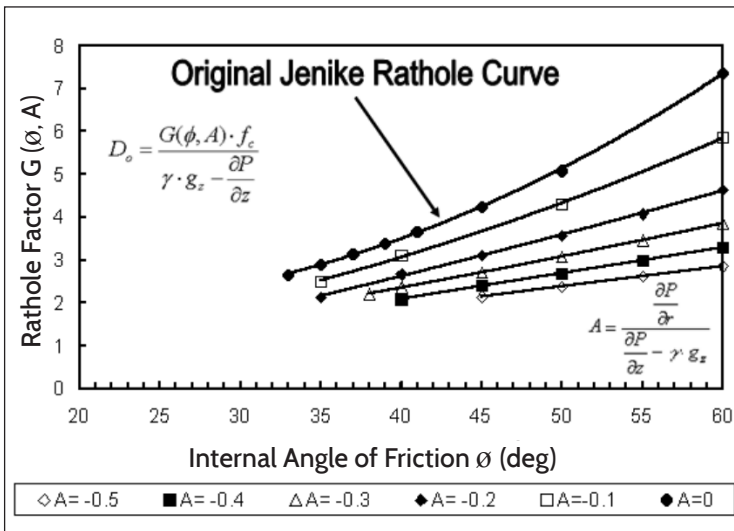


Figure 5: Jenike G factor as a function of internal friction angle (ϕ) at various dimensionless gas pressure gradients (A)

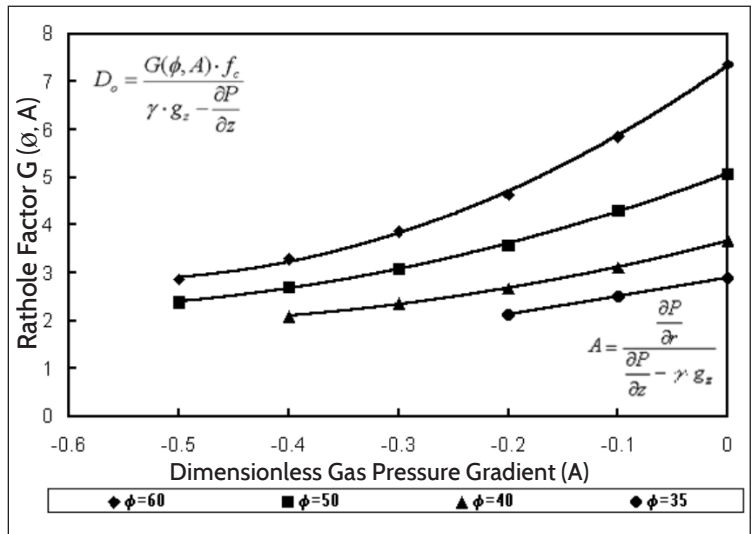


Figure 6: Jenike G factor as a function of dimensionless gas pressure gradient (A) at several internal friction angles (ϕ) between 35E and 60E

Knowledge of the pressure gradients in a bin is required to compute an estimate to the critical rathole dimension. In reality, these gradients are functions of spatial coordinates. This is especially true of the radial pressure gradient. However, an estimate of this radial pressure gradient is obtained by assuming the gas pressure field can be approximated from the solution of a steady state Laplace equation describing permeable materials. If the gas is incompressible, the governing equation is described by Eq. 27.

$$\nabla^2 P = 0 \quad (27)$$

If the gas is subject to isothermal compression, then Eq. 28 applies.

$$\nabla^2 P^2 = 0 \quad (28)$$

For the purposes of this paper, Eq. 27 will be used. If the pressure gradient in the z-direction is constant and the pressure gradient in the θ -direction is small, then Eq. 27 can be expressed simply as a function of the radial coordinate resulting in Eq. 29.

$$\frac{1}{r} \cdot \frac{\partial P}{\partial z} \left[r \cdot \frac{\partial P}{\partial z} \right] = 0 \quad (29)$$

APPLICATION NOTE 013

Normally the gas injection devices used to prevent ratholes are mounted at the bin wall surface. This can be approximated by a constant pressure boundary condition at the bin wall. The pressure at the rathole surface equals the atmospheric pressure. Therefore, Eq. 29 is subject to two constant pressure boundary conditions given in Eq. 30 and Eq. 31.

$$P = P_{\text{atm}} + \Delta P \quad \text{at} \quad r = R_{\text{wall}} \quad (30)$$

$$P = P_{\text{atm}} \quad \text{at} \quad r = R_0 \quad (31)$$

This results in an analytical solution for the gas pressure as a function of radial position (Eq. 32). That solution will yield an equation for the radial gas pressure gradient (Eq. 33) showing an increase in the pressure gradient at the rathole surface.

$$P = \left[\frac{\ln\left(\frac{r}{R_0}\right) - \ln\left(\frac{r}{R_{\text{wall}}}\right)}{\ln\left(\frac{R_{\text{wall}}}{R_0}\right)} \right] \cdot P_{\text{atm}} + \frac{\ln\left(\frac{r}{R_0}\right)}{\ln\left(\frac{R_{\text{wall}}}{R_0}\right)} \cdot \Delta P \quad (32)$$

$$\frac{\partial P}{\partial r} = \frac{1}{r \cdot \ln\left(\frac{R_{\text{wall}}}{R_0}\right)} \cdot \Delta P \quad (33)$$

This can be combined with the definition of the dimensionless radial coordinate (η) given in Eq. 6 and substituted into the dimensionless pressure gradient term (A) found in Eq. 19 to yield a new dimensionless pressure gradient term that depends on the spatial coordinate and the size of the rathole relative to bin diameter (Eq. 34).

$$A(\eta, D_o, D_{\text{wall}}) = \frac{\left[\frac{2 \cdot \frac{\Delta P}{D_{\text{wall}} - D_o}}{\eta^{1/2} \cdot \frac{D_o}{D_{\text{wall}} - D_o} \cdot \ln\left(\frac{D_{\text{wall}}}{D_o}\right)} \right]}{\frac{\partial P}{\partial z} - \gamma \cdot g_z} \quad (34)$$

The new A-value can be used in Eq. 18 to yield a new solution to the rathole equations that incorporates a variable radial pressure gradient. The solution of this equation can then be used in the standard rathole equation. The only difference is that the right side of Eq. 26 now depends on the critical rathole diameter and requires an iterative solution to compute the rathole dimension (Eq. 35).

$$D_o = \frac{G[\phi, A(\eta, D_o, D_{\text{wall}})] \cdot f_c}{\gamma \cdot g_z - \frac{\partial P}{\partial z}} \quad (35)$$

Figure 7 shows the new G-function for the case of an internal angle of friction of 40 degrees as a function of the ratio D_{wall}/D_o and the overall average gas pressure gradient.

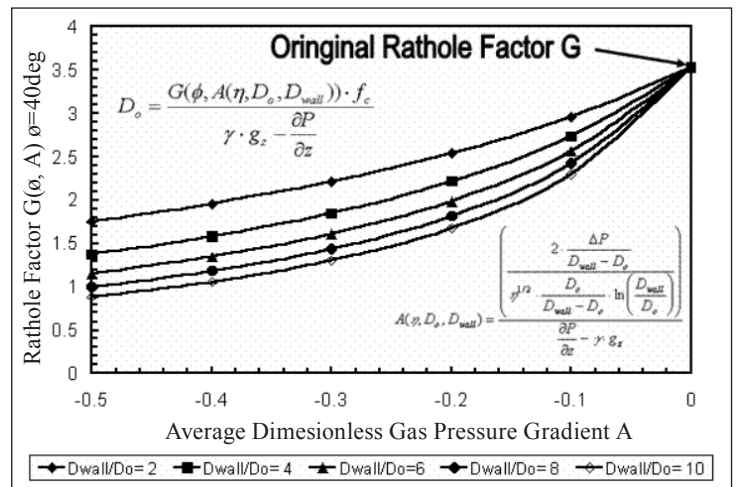


Figure 7: Jenike G-factors for an internal friction angle (ϕ) of 40E as a function of gas pressure gradient at various ratios of bin diameter (D_{wall}) to critical rathole diameter (D_o), D_{wall}/D_o .

The last piece of information required to compute the critical rathole condition in aerated material is an estimate of the unconfined yield strength at aerated conditions and evaluated at solids contact stresses in the process equipment. As indicated previously, researchers have developed testers that measure these aerated cohesive properties as a function of solids contact stresses. These aerated flow functions can be used to estimate the aerated unconfined yield strength needed for this rathole analysis. However, the solids stress in the aerated equipment

APPLICATION NOTE 013

must be known to determine the critical strength value for the rathole analysis. A Janssen analysis of a cylinder with gas effects could be used to estimate the solid contact stresses in a silo. Consider a differential slice of bulk material in a silo (Figure 8).

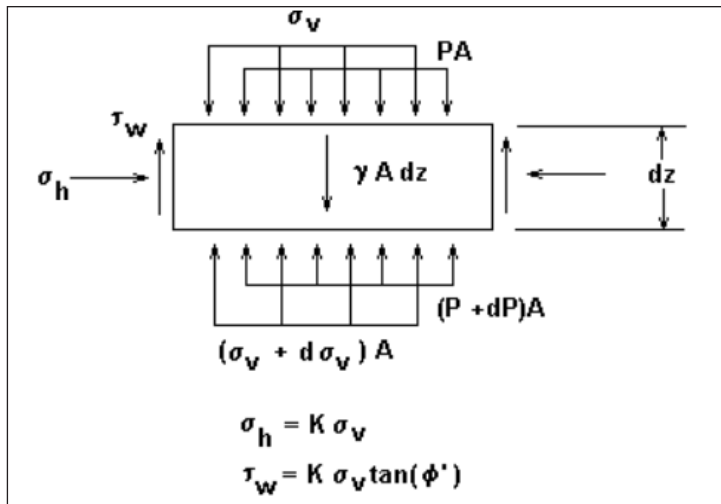


Figure 8: Janssen analysis on aerated material

The forces acting on this differential slice include the solids contact stresses, gas pressures, wall friction, and weight of the material within the slice. A force balance on this differential element results in differential Eq. 36.

$$\frac{d\sigma_v}{dz} + \left[\frac{4 \cdot K \cdot \tan(\phi_w)}{D} \right] \cdot \sigma_v = \gamma \cdot g_z - \frac{\partial P}{\partial z} \quad (36)$$

If the gradient in the axial direction is nearly constant, this differential equation can be integrated subject to a zero stress boundary condition at the top material surface to yield Eq. 37 describing the variation of stress as a function of axial distance from the top of the silo.

$$\sigma_v = \frac{\left[\gamma \cdot g_z - \frac{\partial P}{\partial z} \right] \cdot D}{4 \cdot K \cdot \tan(\phi_w)} \cdot \left[1 - \exp\left(-\frac{4 \cdot K \cdot \tan(\phi_w)}{D} \cdot z \right) \right] \quad (37)$$

This stress level could be evaluated at an axial position (z) equal to the height of the silo to determine an estimate of the solids contact stress for evaluation of the critical rathole diameter in silo geometries. This equation for the solid stress profile in the axial direction assumes that the gas pressure profile is linear along the height of the silo. For conditions where the axial gas pressure gradient varies with time, the most positive axial gas pressure gradient should be used to produce the more conservative solids contact stress for rathole calculations. Eq. 37 should not be used in situations where the gas pressure gradient varies significantly with axial position. It should also be noted that gas pressure gradients in excess of the unit weight density will predict negative solids contact stresses. If this situation occurs, the gas pressure gradient is large enough to cause fluidization of the bulk material provided it is free flowing, or to develop channels with cohesive materials. In either case, the operation mode deviates from the homogenous contact bed conditions inherent in the Janssen stress field assumptions. The solids contact stress should be artificially set equal to zero along the length of the rathole. The procedure for computing the critical rathole dimension in aerated equipment is as follows:

- Estimate the axial gas pressure in the silo.
- Estimate the maximum solids contact stress in the silo with this gas pressure gradient. An accurate approximation to these stresses will require solving both the equations of motion for the gas and solid along with the continuity equations. A Janssen analysis with gas pressure gradient terms may provide an estimate of the critical stress level in the bin.
- Estimate the radial gas pressure gradient in the silo near the rathole surface.
- Estimate the strength of the bulk material at the maximum value of the aerated solids contact stress using the results of the aerated strength test.
- Estimate the $G(\phi, A)$ function from Figure 4 or 6 using the axial and radial estimates of the gas pressure gradients. (A) is the dimensionless gas pressure gradient term which includes the axial and radial gas pressure gradients.
- Use the above equations to compute the critical rathole diameter for the particular geometry.

A numerical example may help to illustrate this procedure. Consider the simple case where the local gas pressure gradients are approximately constant. Please note that this condition may not be the exact condition in aerated bins. Actual pressure

APPLICATION NOTE 013

gradients will depend on the position in the silo. Suppose the conditions and flow properties given in Table I apply to the silo.

Table I: Flow properties and conditions for rathole calculation example

Property or Aeration Condition	Numerical Value
Bulk density (γ)	960 kg/m ³
Radial gas pressure gradient (MP/Mr), (MP/Mr / $\gamma g = 0.4$)	3.76 kPa/m
Axial gas pressure gradient (MP/Mz), (MP/Mz / $\gamma g = 0.05$)	0.47 kPa/m
Internal friction angle (ϕ) assumed to be constant and not a function of gas pressure gradient or solid contact stress	40 degrees
Wall friction angle on silo wall (ϕ_w)	20 degrees
Silo Diameter (D)	5 meters
Silo Height (z)	15 meters
Silo Janssen K-ratio	0.4

One of the important conclusions of previous work done by Barletta [4], Johanson and Barletta [5], and Kline et. al. [6] is that the unconfined yield strength does not change much if the pressure gradient is below some critical value near the fluidization limit. This implies that cohesive flow properties in slightly aerated conditions could be approximated by the measured flow properties in non-aerated conditions. However, this is not true for conditions near fluidization and at conditions in converging conical funnel flow geometries. Thus, for the purposes of this example, the influence of aeration on the critical rathole dimension in cylindrical geometries and pressure gradients less than those required for fluidization will be investigated. The procedure could be applied to more complex situations but the additional complexity would cloud the clarity of this example. Suppose, for the sake of example, that the aerated unconfined yield strength could be expressed as a function of major principal stress described in Figure 9.

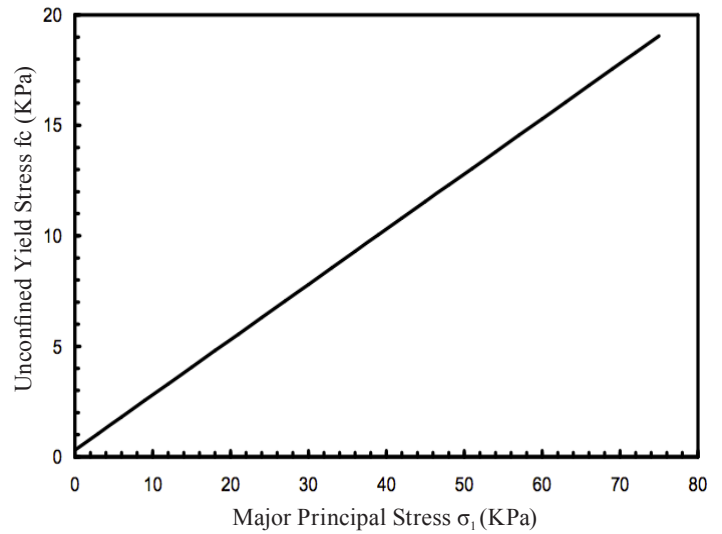


Figure 9: Flow function of aerated material for example rathole calculations

The first step in the procedure above is to estimate the solids stress in the silo using Eq 37. This analysis suggests that the flow properties for rathole analysis should be evaluated at a stress of 63.4 kPa. It is important to point out that this stress is an estimate of the largest major principal stress in the silo over the storage and filling history for the particular silo. This aerated stress would apply for the case where aeration was used on the silo during filling to keep material in a flowable condition. It would not apply to the case where the silo was filled and the aeration system was then turned on in an intermittent mode. The overall maximum solids stress for the intermittent or on-demand gas injection condition would be closer to the non-aerated stress conditions. In fact, processes that use aeration to control the flowability of bulk materials have observed that flow problems arise if the material within the silo becomes deaerated just once. These cohesive deaerated materials are then very difficult to re-aerate and result in persistent rathole problems. It is hoped that this paper will help explain some of these industrial observations.

Once the maximum stress state in the aerated silo is determined the critical strength for rathole calculation can be evaluated using the flow function for the particular aeration condition. In this simple example, the effect of small to moderate gas pressure gradient on the critical rathole dimension are examined and the flow function that applies is the non-aerated condition given in Figure 9. This implies that at a solids stress level of 63.4 kPa the critical strength value for stable rathole formation equals 16.1 kPa. The last step in this

APPLICATION NOTE 013

simplified calculation of aerated critical rathole dimension is to determine the dimensionless gas pressure gradient ratio (A) as given by Equation 19 for constant gradient conditions. This pressure gradient ratio (A) equals -0.421 for the conditions given in Table 1. Figure 6 can then be used to determine the critical rathole factor G used to compute the critical rathole dimension from Equation 26. The entire procedure then yields 3.73 m for the aerated critical rathole dimension. The corresponding critical rathole dimension for non-aerated conditions is 6.59 m suggesting that the assumed aeration conditions for this example case will decrease the rathole tendency to almost half the value of the non-aerated rathole dimension. Thus, controlling the aeration to conditions in this example bin could significantly reduce the size of the active flow channel needed to overcome stable rathole formation. It is important to point out that in this example the critical rathole dimension for non-aerated conditions was greater than the diameter of the bin. This implies that steps must be taken to expand the active flow channel to the full bin diameter to prevent stable rathole formation. If aeration is used then mass flow must only be induced up to the 3.73 m diameter and partial mass flow designs with controlled aeration could be used. This may produce some cost savings in the required bin design.

A similar analysis could be done for the case where gas pressure gradients are a function of radial position. In this case, equation 34 should be used for a calculation of the dimensionless gas pressure gradient (A). In this situation, the A term depends on the critical rathole diameter and will require iteration using equations 34 and 35 to obtain a solution to the critical rathole diameter.

A parametric study of the influence of pressure gradients on rathole stability can be done using the example data in Table 1 and Figure 9 to show the qualitative behavior including gas pressure gradient terms in the rathole limiting stress state equations. Figure 10 shows the expected behavior using the example data. The rathole reduction factor is found by dividing the computed rathole dimension from the analysis above by the standard nonaerated critical rathole dimension from the Jenike method. The strength values needed for this analysis were taken from the example flow function given in Figure 9. This figure indicates that rathole stability can decrease to about 60% of the non-aerated value depending on the radial and axial pressure gradients.

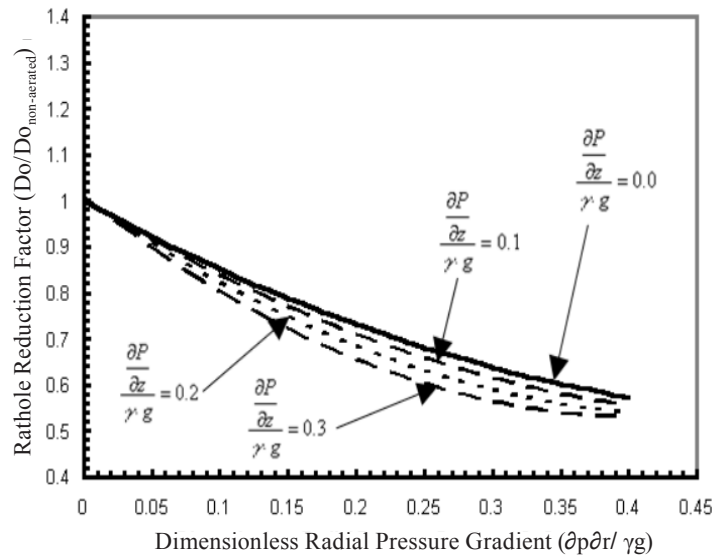


Figure 10: Rathole reduction factor as a function of radial and axial gas pressure gradient using example parameters given in Table 1 and assuming constant gas pressure gradients and the flow function behavior given in Figure 9

Conclusions

The rathole analysis presented in this paper extends the Jenike analysis to aerated conditions. The resulting theory predicts a decrease in the critical rathole diameter as gas pressure gradients acting in the negative r-direction increase. This is intuitively reasonable since the support of ratholes originates in the z-direction. Normal stresses perpendicular to this direction can provide additional body forces required to fail these circumferential cohesive arches (i.e. ratholes). However, increasing the gas pressure gradient in the z-direction will increase the stability of the rathole. This occurs because the upward acting axial gas pressure gradient partially supports the material weight making the material behave as if it were lighter than expected. If the cohesion is the same then lighter material will produce smaller solids contact stresses and result in less stress available to break or destabilize ratholes. The net result is to create more stable ratholes with axial gas counter-flow. Flow aid devices designed to maximize radial gas pressure gradients may overcome rathole problems provided they are placed close to the rathole free surface. This paper provides some preliminary theoretical guidance in using aeration devices to overcome stable rathole formation in process equipment. It is hoped that this work can be refined through Experimental confirmation and industrial observation of rathole stability which will be a subject of future work.

APPLICATION NOTE 013

Nomenclature:

A Dimensionless pressure gradient body force ratio.

D Bin diameter as a function of axial position

D_o Critical rathole diameter

D_{wall} Cylindrical bin diameter

f_c Unconfined yield strength

$G(\varphi, A)$ Critical rathole G factor

H The projected linear yield locus normal tensile stress

K Janssen k-value ratio of stress normal to the wall to the vertical stress in the axial direction. Typically equals 0.4

P Gas pressure

P_{atm} Gas pressure at rathole surface

ΔP Difference between gas pressure at bin wall and gas pressure at rathole surface

r Radial position

R_o Radial position of rathole surface

R_{wall} Radial position of bin wall

γ Powder bulk density

η Dimensionless radial position

η_{max} Maximum value of the dimensionless radius that will produce a stable plastic field

φ Internal friction angle

φ_w Wall friction angle

σ_r Normal stress on the plane perpendicular to the radial direction in a cylindrical coordinate system

σ_θ Normal stress on the plane perpendicular to the direction in a cylindrical coordinate system

σ_z Normal stress on the plane perpendicular to the axial direction in a cylindrical coordinate system

σ Mean limit stress

σ_1 Major principal stress

σ_3 Minor principal stress

σ_v Average vertical stress for Janssen analysis

σ_h Stress normal to cylinder wall for Janssen analysis

τ_{rz} Shear stress on the plane perpendicular to the radial direction acting in the axial direction in a cylindrical coordinate system

$\tau_{r\theta}$ Shear stress on the plane perpendicular to the radial direction acting in the θ -direction in a cylindrical coordinate system

$\tau_{\theta z}$ Shear stress on the plane perpendicular to the θ -direction acting in the axial direction in a cylindrical coordinate system

τ_w Shear stress on the wall for Janssen analysis

ω Angle between the minor principal stress and the r-coordinate direction

Acknowledgment:

The author would also like to acknowledge the financial support of the Engineering Research Center (PERC) for Particle Science and Technology at the University of Florida, the National Science Foundation NSF Grant #EEC-94-02989, and the Industrial Partners of the PERC.

APPLICATION NOTE 013

References:

[1] Jenike, A.W. Gravity flow of bulk solids. Bulletin108, Utah Engineering Station, 1961

[2] Drescher A. Analytical Methods in Bin Loads Analysis, Elsevier; New York, 1991

[3] Johanson J.R., Flow Indices in the Prediction of Powder Behavior, Pharmaceutical Manufacturing International, pp 159-164, 1995

[4] Barletta D., Discharge of fine granular materials from aerated hoppers, Dottorato Di Ricerca In Ingegneria Chimica, University of Salerno, 2002

[5] Johanson K.D. and Barletta D., The Influence of Air Counter-Flow Through Powder Materials on the Measurement of Unconfined Yield Strength, Proceedings of the 4th International Conference for Conveying and Handling of Particulate Solids, 2003

[6] Klein, J., Höhne, D. and Husemann, K. The influence of air permeation on the flow properties of bulk solids. Chem. Eng. Technol. 26 139-146, 2003

[7] Hill, J.M. and Cox, G.M., Cylindrical cavities and classical rat-hole theory occurring in bulk materials, Int. J Numer. Anal. Meth. Geomech., 24:971-990, 2000

[8] Janssen, H. A. Versuche über getreidedruck in silozellen. Z. Ver.Dt. Ing. 39 1045- 1049, 1895